Effect of liquid temperature on sonoluminescence

Kyuichi Yasui
National Institute of Advanced Industrial Science and Technology, 1-1 Hirate-cho, Kita-ku, Nagoya 462-8510, Japan
(Received 9 March 2001; published 18 June 2001)

Computer simulations of bubble oscillations are performed under conditions of sonoluminescence (SL) in water for various liquid temperatures. It is clarified that at almost all acoustic amplitudes, the bubble temperature at the collapse is higher in a colder liquid because a lesser amount of water vapor is trapped inside a bubble at the collapse due to the lower-saturated vapor pressure. Accordingly, at relatively low-acoustic amplitudes, the SL emissions from plasma inside a bubble are much stronger in a colder liquid. However, at higher-acoustic amplitudes, the SL emission originates in chemiluminescence of OH and the intensity is smaller in a colder liquid because a lesser amount of excited OH radicals are created inside a bubble. In actual experiments of multibubble sonoluminescence (MBSL) in water, the light consists of plasma emissions from low-acoustic amplitude region and chemiluminescence of OH from high-acoustic amplitude region. Usually, MBSL in a colder liquid is stronger because of the much stronger plasma emissions. The liquid-temperature dependence of single-bubble sonoluminescence is also discussed.

DOI: 10.1103/PhysRevE.64.016310 PACS number(s): 78.60.Mq

I. INTRODUCTION

When a liquid is irradiated by a strong ultrasound, many tiny gas bubbles appear, which is called acoustic cavitation [1]. The bubbles emit light at the collapse, which was discovered about 70 years ago and is called multibubble sonoluminescence (MBSL) [1,2]. Single-bubble sonoluminescence (SBSL) is a light-emission phenomenon from a stably oscillating bubble trapped at the pressure antinode of a standing ultrasound, which has been studied intensively for a decade [3]. Both for MBSL and SBSL, it has been reported that the light intensity increases as the liquid temperature decreases [4–8]. However, the mechanism of the liquid-temperature dependence is still unclear [1,4,9,10]. In the present paper, it is investigated by computer simulations of bubble oscillations both for MBSL and SBSL.

II. MODEL

For the bubble collapse under SL conditions, there are two theoretical models; the shock-wave model [11,12] and the quasiadiabatic compression model [13]. The shock-wave model [11,12] is that a spherically symmetric shock wave develops inside the bubble at the collapse and converges at the bubble center. The quasiadiabatic compression model [13] is that no shock-wave develops inside the bubble and the whole bubble is heated up by the quasiadiabatic compression (''quasi'' means that appreciable thermal conduction takes place between the bubble and the surrounding liquid). In 1998, Cheng *et al.* [14,15] showed by the computer simulations of the fundamental equations of fluid dynamics inside a collapsing bubble that no shock wave is formed inside a SL bubble and the spatial-variations of temperature and pressure inside a bubble are both only a few tens of percent. The reason for no shock formation was theoretically clarified by Vuong, Szeri, and Young in 1999 [16]. Thus, in the present computer simulations, a quasiadiabatic compression model [13] is used.

In the present model, the effect of nonequilibrium evaporation and condensation of water vapor at the bubble wall, of thermal conduction both inside and outside a bubble, of chemical reactions of gases and vapor inside a bubble, of ionization of gases inside a bubble, and of liquid compressibility are taken into account. The present model is basically the same as that described in Ref. [13] except a few modifications.

As in Ref. [13], it is assumed that the pressure and the temperature are spatially uniform inside a spherical bubble except at the thermal boundary layer near the bubble wall. The thickness of the thermal boundary layer is $n\lambda$ where n is a constant ($n=7$) and λ is a mean free path of molecules inside a bubble [13,17].

As the equation of bubble radius (R), the modified Keller equation is used.

$$\left(1-\frac{\dot R}{c_\infty}+\frac{\dot m}{c_\infty\rho_{L,i}}\right)R\ddot R+\frac{3}{2}\dot R^2\left(1-\frac{\dot R}{3c_\infty}+\frac{2\dot m}{3c_\infty\rho_{L,i}}\right)$$
$$=\frac{1}{\rho_{L,\infty}}\left(1+\frac{\dot R}{c_\infty}\right)\left[p_B-p_s\left(t+\frac{R}{c_\infty}\right)-p_\infty\right]+\frac{\ddot m R}{\rho_{L,i}}\left(1-\frac{\dot R}{c_\infty}+\frac{\dot m}{c_\infty\rho_{L,i}}\right)+\frac{\dot m}{\rho_{L,i}}\left(\dot R+\frac{\dot m}{2\rho_{L,i}}+\frac{\dot m\dot R}{2c_\infty\rho_{L,i}}-\frac{R}{\rho_{L,i}}\frac{d\rho_{L,i}}{dt}-\frac{\dot m R}{c_\infty\rho_{L,i}^2}\frac{d\rho_{L,i}}{dt}\right)+\frac{R}{c_\infty\rho_{L,\infty}}\frac{dp_B}{dt},\qquad(1)$$

where the dot denotes the time derivative (d/dt), c_∞ is the sound speed in the liquid at infinity, $\dot m$ is the rate of evaporation of water at the bubble wall per unit area per unit time, $\rho_{L,i}$ ($\rho_{L,\infty}$) is the liquid density at the bubble wall (at infinity), $p_B(t)$ is the liquid pressure on the external side of the bubble wall, $p_s(t)$ is a nonconstant ambient pressure component such as a sound field, and p_∞ is the undisturbed pressure. When a bubble is irradiated by an acoustic wave whose wavelength is much larger than the bubble radius, $p_s(t)=-p_a\sin(2\pi f_a t)$ where p_a is the pressure amplitude of the

acoustic wave and f_a is its frequency. By the fundamental theory of fluid dynamics [18], it can be shown that the speed of the bubble collapse never exceeds the sound velocity of the liquid *at the bubble wall* ($c_{L,B}$) (see Appendix), which is a function of the liquid pressure at the bubble wall (p_B); $c_{L,B}=\sqrt{7.15(p_B+B)/\rho_{L,i}}$ where $B=3.049\times10^8$ Pa and $\rho_{L,i}$ is the liquid density at the bubble wall [19]. Thus, in the present computer simulations, the bubble wall velocity is replaced by $c_{L,B}$ when it exceeds $c_{L,B}$ in the numerical calculations of the modified Keller equation, which is the most important modification in the present model.

The change of the thermal energy of a bubble (ΔE) in time Δt is expressed by

$$\Delta E(t)=-p_g(t)\cdot\Delta V(t)+4\pi R^2\dot{m}e_{\mathrm{H_2O}}\Delta t + 4\pi R^2\Delta t\cdot\kappa\left.\frac{\partial T}{\partial t}\right|_{r=R}+\frac{4}{3}\pi R^3\Delta t\sum_{\gamma}\left(r_{\gamma b}-r_{\gamma f}\right)\times\Delta H_{\gamma f}+\left[-\frac{3}{5}M\dot{R}\ddot{R}\right]\Delta t-\sum_i\chi_{\mathrm{red},i}\Delta n_i^+, \quad (2)$$

where p_g is the pressure inside a bubble, ΔV is the volume change of the bubble, R is the bubble radius, $\dot{m}$ is the rate of evaporation of water at the bubble wall, $e_{\mathrm{H_2O}}$ is the energy carried by an evaporating or condensing vapor molecule, κ is the thermal conductivity of the gas, $\left.\partial T/\partial r\right|_{r=R}$ is the temperature gradient at the bubble wall, $r_{\gamma f}(r_{\gamma b})$ is the forward (backward) reaction rate of the reaction γ per unit volume and unit time, $\Delta H_{\gamma f}$ is the enthalpy change in the forward reaction (when $\Delta H_{\gamma f}<0$, the reaction is exothermic), M is the total mass of the gases and vapor inside the bubble, the dot denotes the time derivative (d/dt), $\chi_{\mathrm{red},i}$ is the reduced ionization potential of the gas species i by the extreme high density, and Δn_i^+ is the change of the number of positive ions of the species i. The first term in the right-hand side of Eq. (2) is the work by pressure (pV work). The second term is the energy carried by evaporating or condensing vapor molecules. The third term is the energy change due to thermal conduction. The fourth term is the heat of chemical reactions inside the bubble. The fifth term is the change of the macroscopic kinetic energy of the gas that is transferred to heat [13]. The brackets mean that this term is included only when the term is positive, which corresponds to the decrease of the kinetic energy. When the term is negative, it is replaced by zero. The last term is the heat of ionization. As has been clarified in the previous studies [13,17], the heat of chemical reactions, especially the endothermal heat of vapor dissociation, affects the bubble temperature considerably.

The molar heat (C_V) of gases and vapor inside an argon bubble is

$$C_V=\frac{3}{2}R_g\frac{n_{\mathrm{Ar}}}{n_t}+\frac{6}{2}R_g\frac{n_{\mathrm{H_2O}}}{n_t}+\sum_i C_{V,i}\frac{n_i}{n_t}-\left(\frac{n_t}{N_A}\right)^2\frac{a}{V}, \quad (3)$$

where R_g is the gas constant, n_{Ar} is the number of argon atoms inside a bubble, n_t is the total number of particles inside a bubble, $n_{\mathrm{H_2O}}$ is the number of water-vapor molecules inside a bubble, $C_{V,i}$ is the molar heat of the gas species i ($i=$OH, H, O, O_2, H_2, HO_2, H_2O_2, O_3), n_i is the number of molecules of the gas species i inside a bubble, N_A is the Avogadro number, a is the van der Waals constant, and V is the bubble volume [13]. The molar heat of the gas species i is assumed as follows; for monoatomic gases such as H and O, the molar heat is $(3/2)R_g$, for diatomic gases such as OH, O_2, H_2, it is $(5/2)R_g$, for the other gases, it is $(6/2)R_g$ [20]. As has been clarified previously [13,17], the second term, which is determined by the number of water-vapor molecules inside a bubble, affects the bubble temperature at the collapse considerably.

The thermal conductivity (κ) of the gas inside a bubble is estimated by Eq. (4):

$$\kappa=\kappa_{\mathrm{H_2O}}(T)(n_{\mathrm{H_2O}}/n_t)+\kappa_{\mathrm{Ar}}(T)(n_{\mathrm{Ar}}/n_t), \quad (4)$$

where $\kappa_{\mathrm{H_2O}}(T)$ and $\kappa_{\mathrm{Ar}}(T)$ are the thermal conductivity of water vapor and that of argon at temperature T, respectively. The thermal conductivity of water vapor and that of argon are estimated by $\kappa_{\mathrm{H_2O}}(T)=-0.012+1.0\times10^{-4}T$ and $\kappa_{\mathrm{Ar}}(T)=0.009+3.2\times10^{-5}T$, where $\kappa_{\mathrm{H_2O}}$ and κ_{Ar} are in W/m K and T is the temperature in K.

Another modification made in the present model is the inclusion of the dissolution of chemical products such as OH, O, H, etc. into water. The rate of dissolution (r_d) is calculated for each species by the following equation:

$$r_{d,i}=\Theta\sqrt{\frac{kT_B}{2\pi m_i}}\frac{n_i}{V}\times4\pi R^2, \quad (5)$$

where $r_{d,i}$ is the rate of dissolution of the chemical species i ($i=$OH, H, O, O_2, H_2, O_3, HO_2, H_2O_2), Θ is the probability of dissolution of a molecule per collision to the liquid surface ($\Theta=0.001$ [21]), k is the Boltzmann constant, T_B is the gas temperature at the bubble wall, m_i is the molecular mass of the species i, n_i is the number of molecules of the species i inside a bubble, V is the bubble volume, and R is the bubble radius.

Now, we discuss the ionization of gases inside a bubble. In dense gas, the ionization potential of the gas is reduced by the overlap of the electron wave functions of gas molecules [22,23]. The reduced ionization potential (χ_{red}) is estimated by Eq. (6) [22,23]:

$$\chi_{\mathrm{red}}=\chi(1-1/x), \quad (6)$$

where

$$x=\frac{1}{2a_Bk'}\sqrt[3]{\frac{V}{n_t}}, \quad (7)$$

χ is the ionization potential of the gas in vacuum, a_B is the Bohr radius (5.29×10^{-11} m), k' is the ratio of the atomic radius of the gas to that of hydrogen ($k'=1.57$ for argon, and 1.27 for oxygen atom), V is the bubble volume, and n_t is the total number of molecules inside a bubble.

In the present calculations, the ionization of argon, oxygen, and hydrogen atoms are taken into account because al-

most all water-vapor molecules are dissociated to oxygen and hydrogen atoms when ionization takes place [13]. The ionization potential of argon in vacuum is 15.8 eV and those of oxygen and hydrogen atoms in vacuum are both 13.6 eV. The number of free electrons (n_e) is estimated by Saha equation [24].

$$n_e=\frac{V}{2}\left[-\lambda_e^{-3}e^{-\overline{\chi}/kT}+\sqrt{(\lambda_e^{-3}e^{-\overline{\chi}/kT})^2+4\lambda_e^{-3}(n_{\mathrm{Ar}}e^{-\chi_{\mathrm{red,Ar}}/kT}+n_{\mathrm{O}}e^{-\chi_{\mathrm{red,O}}/kT}+n_{\mathrm{H}}e^{-\chi_{\mathrm{red,H}}/kT})/V}\right], \tag{8}$$

where V is the bubble volume, $\lambda_e=h/\sqrt{2\pi m_e kT}$ is the thermal de Broglie wavelength of electrons, h is the Planck constant, m_e is the electron mass, k is the Boltzmann constant, T is the temperature, $\overline{\chi}$ is the averaged ionization potential over the species considered, n_{Ar} is the number of argon atoms inside the bubble, $\chi_{\mathrm{red,Ar}}$ is the reduced ionization potential of argon, n_{O} and n_{H} are the numbers of oxygen and hydrogen atoms inside the bubble, respectively, and $\chi_{\mathrm{red,O}}$ and $\chi_{\mathrm{red,H}}$ are the reduced ionization potentials of oxygen and hydrogen atoms, respectively. The number of positive ions of the species i (n_i^+) is calculated by Eq. (9):

$$n_i^+=n_i y/(n_e+y), \tag{9}$$

where

$$y=\lambda_e^{-3}e^{-\chi_{\mathrm{red},i}/kT}\times\tfrac{4}{3}\pi R^3, \tag{10}$$

n_i is the number of atoms of the species i including both neutrals and ions and $\chi_{\mathrm{red},i}$ is the reduced ionization potential of the species i.

In the present paper the radiative processes are also simulated. The processes include chemiluminescence of OH, plasma emissions, and the thermal emissions of O_2 molecules. For chemiluminescence and O_2 emissions, the quenching by collisions with other particles is taken into account by multiplying the factor $1/[1+\Sigma_i\pi\sigma_i^2\tau\overline{v_i}(n_i/V)]$ [25] where $\pi\sigma_i^2$ is the quenching cross section of the species i ($\pi\sigma_i^2=2.1\times10^{-21}(\mathrm{m}^2)$ for argon, $3.5\times10^{-19}(\mathrm{m}^2)$ for H_2O, $7\times10^{-20}(\mathrm{m}^2)$ for the other molecules [26]), τ is the lifetime of the excited OH radicals ($\tau=7\times10^{-7}$ s [26]), $\overline{v_i}$ is the mean velocity of the molecules of the species i, n_i is the number of molecules of the species i inside a bubble, and V is the bubble volume. The intensity of the chemiluminescence from OH* is estimated by the rates of the reactions O+H+M→OH*+M (OH* is the excited OH radical and M is the third body) and OH+H+OH→OH*+H_2O [13,27,28] multiplied by the quenching factor.

The plasma emissions consist of electron-ion bremsstrahlung, electron-atom bremsstrahlung, radiative recombination of electrons and ions, and radiative attachment of electrons to neutral particles. The electron-ion bremsstrahlung is the light emission from an electron accelerated in the Coulomb field of a positive ion and the intensity is given by Eq. (11).

$$P_{\mathrm{Br,ion}}=1.57\times10^{-40}n_e^2T^{1/2}/(\tfrac{4}{3}\pi R^3), \tag{11}$$

where n_e is the number of electrons inside a bubble, T is the temperature, R is the bubble radius, and all the quantities are expressed in SI units. The electron-atom bremsstrahlung is the light emission from an electron accelerated in the field of a neutral atom and the intensity is crudely estimated by Eq. (12) [29]:

$$P_{\mathrm{Br,atom}}=4.6\times10^{-44}n_e n_{\mathrm{Ar}}T/(\tfrac{4}{3}\pi R^3), \tag{12}$$

where all the quantities are expressed in SI units.

The intensity of radiative recombination (P_r) is estimated by

$$P_r=n_e^2\langle\sigma_{fb}v_e\rangle h\overline{\nu}/(\tfrac{4}{3}\pi R^3), \tag{13}$$

where σ_{fb} is the cross section of radiative recombination, v_e is the velocity of a free electron, $\langle\ \rangle$ denotes the averaged value over the Maxwell-Boltzmann velocity distribution, and $h\overline{\nu}$ is the mean energy of the emitted photon ($h\overline{\nu}=1.5\,kT$). According to Ref. [30], $\langle\sigma_{fb}v_e\rangle=2.7\times10^{-17}/\sqrt{T}$ (m^3/s) for hydrogen, where T is expressed in K. For argon and oxygen, the detailed values of σ_{fb} are not known. Thus, in the present calculations, the value of hydrogen is used.

The intensity of radiative attachment of electrons to the neutral oxygen atoms is given by Eq. (14) [31]:

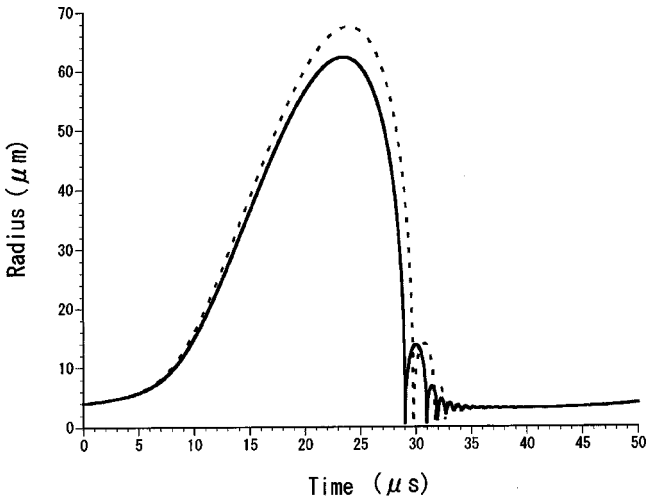

FIG. 1. The calculated radius-time curves of an argon bubble for one acoustic cycle (50 μs) for the liquid temperature of 20 °C (solid line) and 34 °C (dotted line) when the frequency and the amplitude of ultrasound are 20 kHz and 1.4 bar, respectively, and the ambient bubble radius is 4 μm.

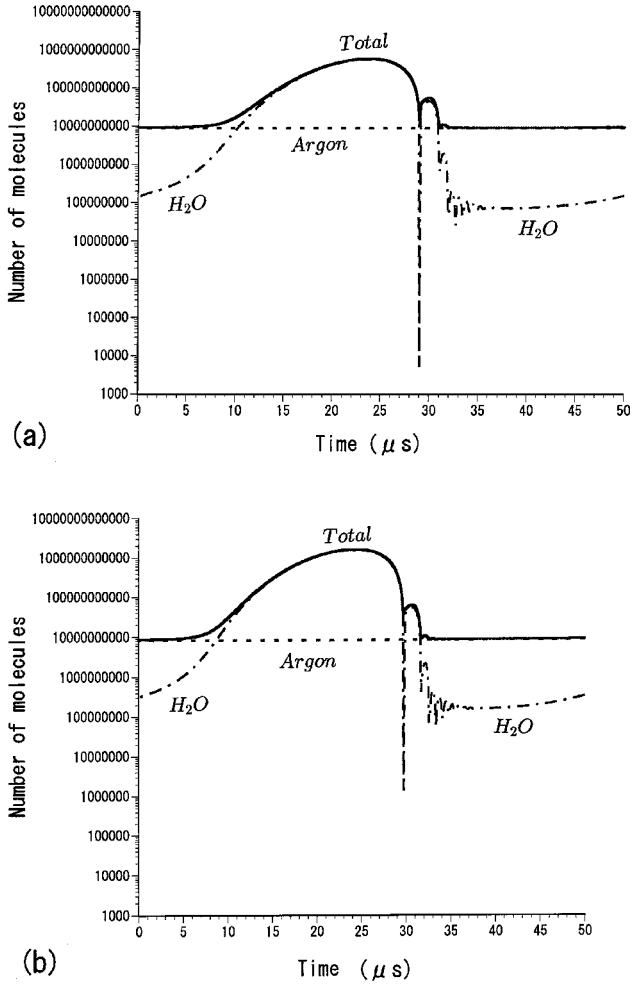

FIG. 2. The numbers of molecules inside a bubble as functions of time for one acoustic cycle for the liquid temperature of 20 °C (a) and 34 °C (b). The condition is the same as that of Fig. 1.

$$P_{\mathrm{att}} = 1\times 10^{-26} n_{\mathrm{O}} n_e \overline{v_e} h\overline{\nu} / (\tfrac{4}{3}\pi R^3), \tag{14}$$

where the coefficient $[1\times 10^{-26}(\mathrm{m}^2)]$ is the cross section of radiative attachment, n_{O} and n_e are the numbers of oxygen atoms and electrons inside a bubble, respectively, $\overline{v_e}$ is the mean velocity of electrons ($\overline{v_e} = \sqrt{8\,kT/\pi m_e}$, where k is the Boltzmann constant, m_e is the electron mass), and $h\overline{\nu}$ is the mean energy of the emitted photon ($h\overline{\nu} = 1.5\,kT$). In the present calculations, the intensity of radiative attachment of electrons to hydrogen atoms, OH radicals, and oxygen molecules are also calculated using the similar equations to Eq. (14).

TABLE I. The physical properties of liquid water for various temperatures. p_v^* is the saturated vapor pressure, μ is the viscosity, ν is the kinematic viscosity, σ is the surface tension, and ρ_L is the density.

	5 °C	20 °C	34 °C
p_v^* (Pa)	0.86×10^3	2.32×10^3	5.29×10^3
μ (Pa s)	1.52×10^{-3}	1.00×10^{-3}	0.74×10^{-3}
ν (m^2/s)	1.52×10^{-6}	1.00×10^{-6}	0.74×10^{-6}
σ (N/m)	7.49×10^{-2}	7.28×10^{-2}	7.05×10^{-2}
ρ_L ($\mathrm{kg/m}^3$)	1.00×10^3	1.00×10^3	0.99×10^3

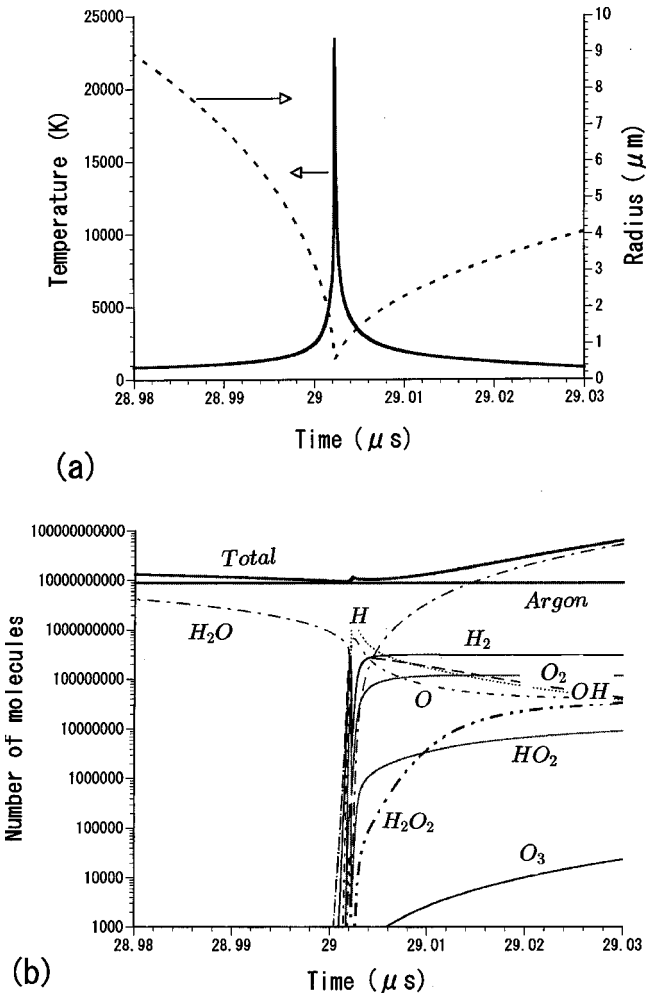

FIG. 3. The calculated results for the liquid temperature of 20 °C at around the minimum bubble radius as functions of time for 0.05 μs. The condition is the same as that of Fig. 1. (a) The bubble radius (R) and the temperature inside the bubble (T). (b) The numbers of molecules inside the bubble.

III. RESULTS

The computer simulations are performed for an argon bubble in water irradiated by 20 kHz ultrasound of various acoustic amplitudes for various liquid temperatures (5, 20, and 34 °C). In Fig. 1, the calculated radius-time curves are shown for one acoustic cycle for 20 °C case (solid line) and 34 °C case (dotted line) when the acoustic amplitude is 1.4 bar and the ambient bubble radius is 4 μm, where the ambient bubble radius is defined as the bubble radius when ultrasound is off. From Fig. 1, it is seen that at 34 °C the bubble expands more compared to 20 °C case. In Fig. 2, numbers of molecules inside a bubble are shown for 20 °C case (a) and 34 °C case (b). It is seen that much more water evaporates into the bubble at the bubble expansion for 34 °C case, which

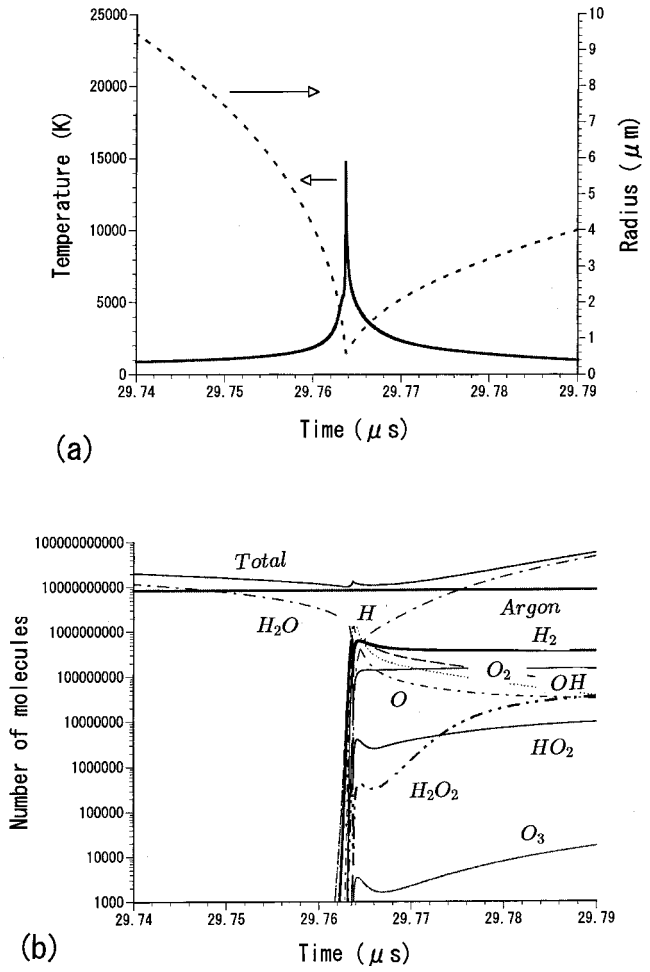

FIG. 4. The calculated results for the liquid temperature of 34 °C at around the minimum bubble radius as functions of time for 0.05 μs. The condition is the same as that of Fig. 1. (a) The bubble radius (R) and the temperature inside the bubble (T). (b) The numbers of molecules inside the bubble.

is due to the larger saturated vapor pressure at 34 °C (Table I). As seen in Fig. 2, the number of water-vapor molecules inside a bubble decreases at the bubble collapse due to the vapor condensation at the bubble wall. It should be noted here that vapor condensation at the bubble wall is a nonequilibrium process due to the high speed of the bubble collapse [32].

In Figs. 3 and 4, the enlarged views at around the minimum bubble radius are shown for 20 and 34 °C cases, respectively. It is seen that the maximum bubble temperature is much higher for 20 °C case. It is because the amount of vapor trapped inside a bubble is much smaller for 20 °C case as seen in Figs. 3(b) and 4(b). Vapor has a larger molar heat $[(6/2)R_g]$ than that of argon $[(3/2)R_g]$. Thus, the bubble with larger amount of vapor needs much more energy for the same temperature increase. It results in the lower maximum temperature of the bubble for 34 °C case as shown in Table II. Additionally, vapor is dissociated inside a bubble at the collapse by the high temperature and cools the bubble considerably due to the endothermal heat of the dissociation, which makes the maximum bubble temperature for 34 °C case much lower than that for 20 °C case as shown in Table II.

TABLE II. The calculated results for an argon bubble in water irradiated by ultrasound of 20 kHz and 1.4 bar for the liquid temperatures of 20 and 34 °C. The ambient bubble radius is 4 μm. R_{max} is the maximum bubble radius, R_{min} is the minimum bubble radius, T_{max} is the maximum bubble temperature, the temperature in the brackets is the maximum bubble temperature when chemical reactions are neglected, ''H_2O dissociated'' is the number of H_2O molecules dissociated inside a bubble per bubble collapse, ''light'' is the energy of the emitted light per bubble collapse, ''pulse width'' is that of the emitted light, ''mechanism'' is that of the light emission, ''rad.rec.'' is radiative recombination of electrons and ions, ''ion bremss.'' is electron-ion bremsstrahlung, ''atom bremss.'' is electron-atom bremsstrahlung, and ''rad. attach.'' is radiative attachment of electrons to neutral particles.

	20 °C	34 °C
R_{max}	62 μm	68 μm
R_{min}	0.6 μm	0.6 μm
T_{max}	24 000 K	15 000 K
(without CR)	(40 000 K)	(36 000 K)
H_2O dissociated	4.5×10^8	4.7×10^8
light	7.4 pJ	0.3 pJ
pulse width	50 ps	40 ps
mechanism	rad. rec.	atom bremss.
	ion bremss.	rad. rec.
	atom bremss.	rad. attach.

In Figs. 5(a), 6(a), and 7(a), the bubble temperature at the collapse is shown for various acoustic amplitudes and ambient radii for the liquid temperatures of 5, 20, and 34 °C, respectively. The ranges of the acoustic amplitudes (p_a) and the ambient radii (R_0) considered are 0–10 bar and 1–6 μm, respectively, which are typical ones in MBSL experiments [1,33]. From Fig. 5(a), it is seen that at first the bubble temperature at the collapse increases as the acoustic amplitude increases up to ~1.5 bar. It is because the bubble collapse becomes more violent as the acoustic amplitude increases. However, above ~1.5 bar, the bubble temperature decreases as the acoustic amplitude increases. The reason is as follows. As the acoustic amplitude increases, a bubble expands more, and more vapor evaporates into a bubble at the expansion. It results in the increase of the amount of vapor trapped inside a bubble at the collapse, and thus, the bubble temperature at the collapse decreases.

Comparing Figs. 5(a), 6(a), and 7(a), it is seen that for almost all acoustic amplitudes, the bubble temperature at the collapse is higher in a colder liquid. The reason is that a lesser amount of vapor is trapped inside a bubble at the collapse in a colder liquid due to the lower-saturated vapor pressure. Although for almost all the acoustic amplitudes the bubble temperature at the collapse is higher in a colder liquid, there exists a very narrow range of acoustic amplitude for which the bubble temperature at the collapse is *lower* in a colder liquid. For example, at $p_a=1.2$ bar and $R_0=4$ μm, it is 7600 K for 20 °C case while it is 11 000 K for 34 °C case. It is because the amount of vapor trapped inside

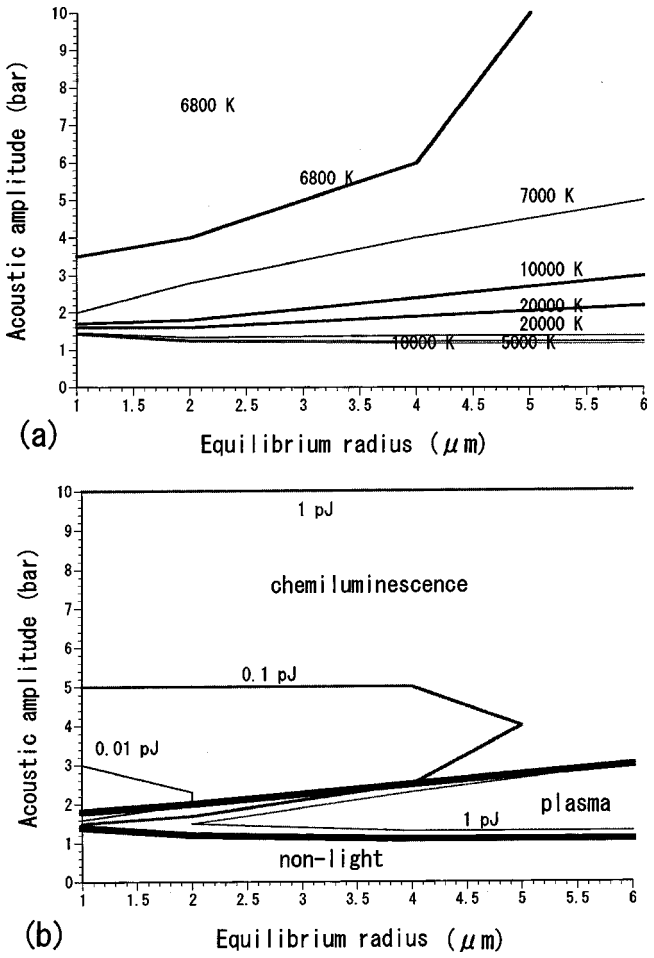

FIG. 5. The calculated results for the liquid temperature of 5 °C when an argon bubble of various ambient radii (R_0) in water is irradiated by 20 kHz ultrasound of various acoustic amplitudes (p_a). (a) The bubble temperature at the collapse. The isothermal lines are from the bottom 5000, 10 000, 20 000, 20 000, 10 000, 7000 and 6800 K. Above the line of 6800 K, the bubble temperature at the collapse is independent of acoustic amplitude and is always 6800 K. (b) Mechanism of the light emission and the energy of the emitted light per bubble collapse.

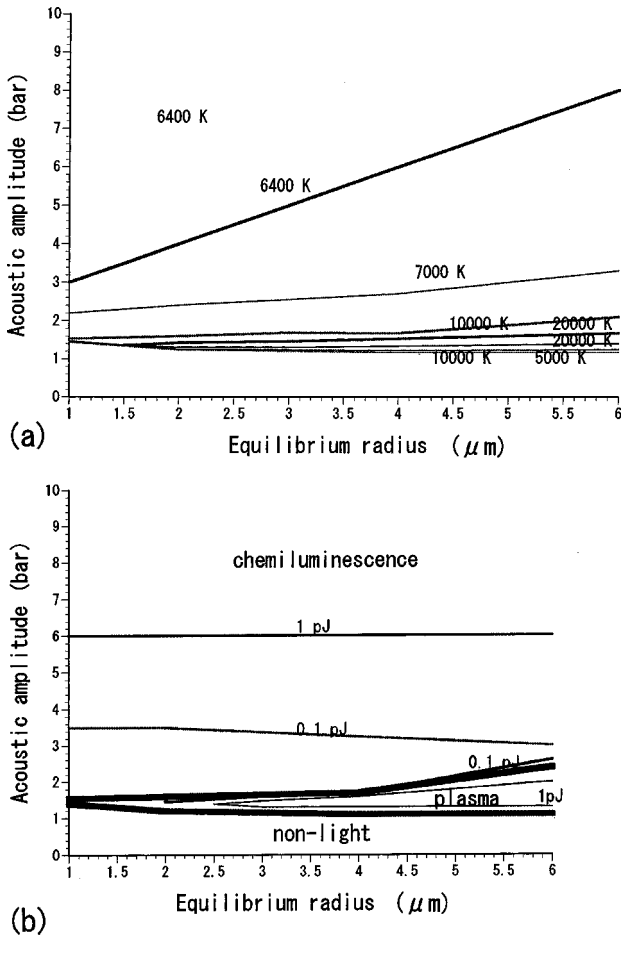

FIG. 6. The calculated results for the liquid temperature of 20 °C when an argon bubble of various ambient radii (R_0) in water is irradiated by 20 kHz ultrasound of various acoustic amplitudes (p_a). (a) The bubble temperature at the collapse. The isothermal lines are from the bottom 5000, 10 000, 20 000, 20 000, 10 000, 7000 and 6400 K. Above the line of 6400 K, the bubble temperature at the collapse is independent of acoustic amplitude and is always 6400 K. (b) Mechanism of the light emission and the energy of the emitted light per bubble collapse.

a bubble is very small, in this case, due to a relatively small expansion of the bubble by the relatively small acoustic amplitude. The main factor that determines the bubble temperature at the collapse in this case is the bubble temperature at the beginning of the collapse, which is identical to the liquid temperature. It should be noted that the expansion of the bubble is an isothermal process and the bubble temperature at the maximum bubble radius is identical to the liquid temperature [34]. Lower-initial temperature results in the lower-final temperature.

In Figs. 5(b), 6(b), and 7(b), the mechanism of the light emission is shown with the energy of the emitted light per bubble collapse for the liquid temperatures of 5, 20, and 34 °C, respectively. At low-acoustic amplitudes it is a plasma emission and at high-acoustic amplitudes, it is chemiluminescence of OH. In actual experiments of multibubble sonoluminescence (MBSL), the acoustic amplitude varies spatially inside a liquid. Thus, MBSL is a combination of plasma emissions from low-acoustic amplitude region and chemiluminescence from high-acoustic amplitude region. Indeed, the MBSL spectra consist of continuum (plasma emissions) and OH line (chemiluminescence) [6,33].

Comparing Figs. 5–7, it is seen that plasma emissions from low-acoustic amplitude region is much stronger in a colder liquid than those in a hotter liquid because the bubble temperature at the collapse is higher. On the other hand, chemiluminescence of OH from a high-acoustic amplitude region is stronger in a hotter liquid than that in a colder liquid because much more vapor is trapped inside a bubble at the collapse and much more excited OH radicals are created. Thus, it is concluded that MBSL from a colder liquid consists of much stronger plasma emissions and a weaker OH emission compared to that from a hotter liquid. The increase of MBSL intensity as the liquid is cooled, which has been reported experimentally [5–8], is due to the strong increase of plasma emissions. Here it should be noted that the number

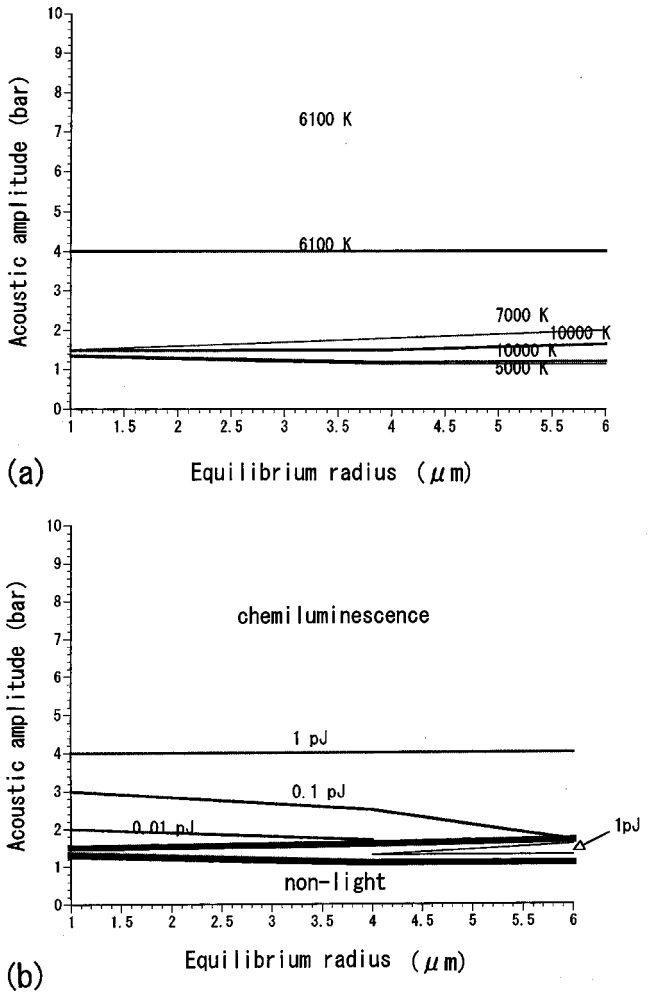

FIG. 7. The calculated results for the liquid temperature of 34 °C when an argon bubble of various ambient radii (R_0) in water is irradiated by 20 kHz ultrasound of various acoustic amplitudes (p_a). (a) The bubble temperature at the collapse. The isothermal lines are from the bottom 5000, 10 000, 10 000, 7000, and 6100 K. Above the line of 6100 K, the bubble temperature at the collapse is independent of acoustic amplitude and is always 6100 K. (b) Mechanism of the light emission and the energy of the emitted light per bubble collapse. At the narrow region between the two thick lines, the light originates in plasma emissions.

of bubbles in a liquid is also a very important factor that determines the intensity of MBSL. In the present paper, the changes of the number of bubbles and their size and spatial distributions are not dealt with.

In Figs. 8–10, examples of the calculated results for a high-acoustic amplitude at which light originates in chemiluminescence are shown. The acoustic amplitude is 5 bar and the ambient bubble radius is 4 μm. In Fig. 8, the calculated radius-time curves are shown for one acoustic cycle for 20 °C case (solid line) and 34 °C case (dotted line). It is seen that a bubble expands much more when compared to the case of the low-acoustic amplitude (Fig. 1). Thus, a much larger amount of vapor evaporates into a bubble at the expansion and the amount of vapor trapped inside a bubble at the collapse in the case of the high-acoustic amplitude [Figs. 9(b) and 10(b)] is much larger than that in the case of the low-

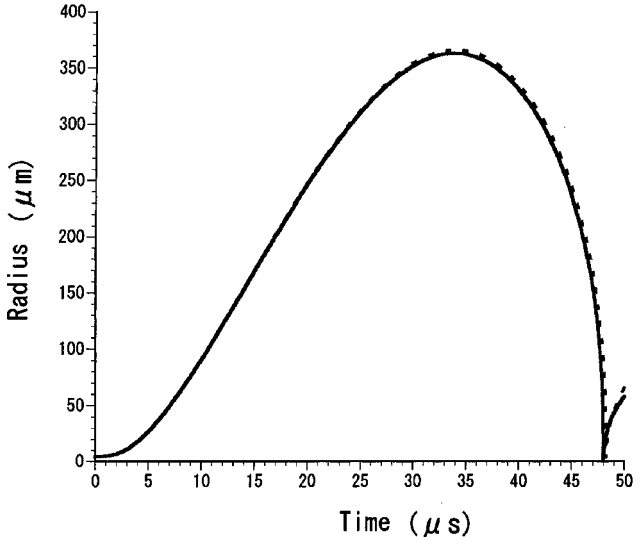

FIG. 8. The calculated radius-time curves for one acoustic cycle (50 μs) for the liquid temperature of 20 °C (solid line) and 34 °C (dotted line) when the frequency and the amplitude of ultrasound are 20 kHz and 5 bar, respectively and the ambient bubble radius is 4 μm. Note the much larger scale of the vertical axis than that of Fig. 1.

acoustic amplitude [Figs. 3(b) and 4(b)]. It results in the much lower bubble temperature at the collapse (T_{max} in Table III) compared to that in the case of the low-acoustic amplitude (Table II). It is also seen from Table III that the bubble temperature at the collapse is higher for 20 °C case compared to 34 °C case because a lesser amount of vapor is trapped inside a bubble at the collapse, as in the case of the low-acoustic amplitude (Table II).

Finally, we discuss the liquid-temperature dependence of single-bubble sonoluminescence (SBSL). In 2000, Vazquez and Putterman [4] reported that the SBSL intensity increases as the liquid temperature decreases under a similar acoustic amplitude. For example, they reported that when the maximum bubble radius is the same (R_{max}=37 μm) the light intensity in 20 °C case is five times larger than that in the 34 °C case. In the present paper, computer simulations are performed under the experimental conditions of Vazquez and Putterman [4]. The calculated results are summarized in Table IV. It is seen that the calculated number of photons emitted per bubble collapse is larger for 20 °C case due to the higher maximum bubble temperature, which is caused by the smaller amount of vapor trapped inside a bubble at the collapse.

IV. CONCLUSION

At almost all the acoustic amplitudes, the bubble temperature at the collapse is higher in a colder liquid. It is because the amount of water vapor trapped inside a bubble at the collapse is smaller due to the lower-saturated vapor pressure. Multibubble sonoluminescence (MBSL) in water is a combination of plasma emissions from low-acoustic amplitude region and chemiluminescence of OH from high-acoustic amplitude region. In a colder liquid, plasma emissions are much

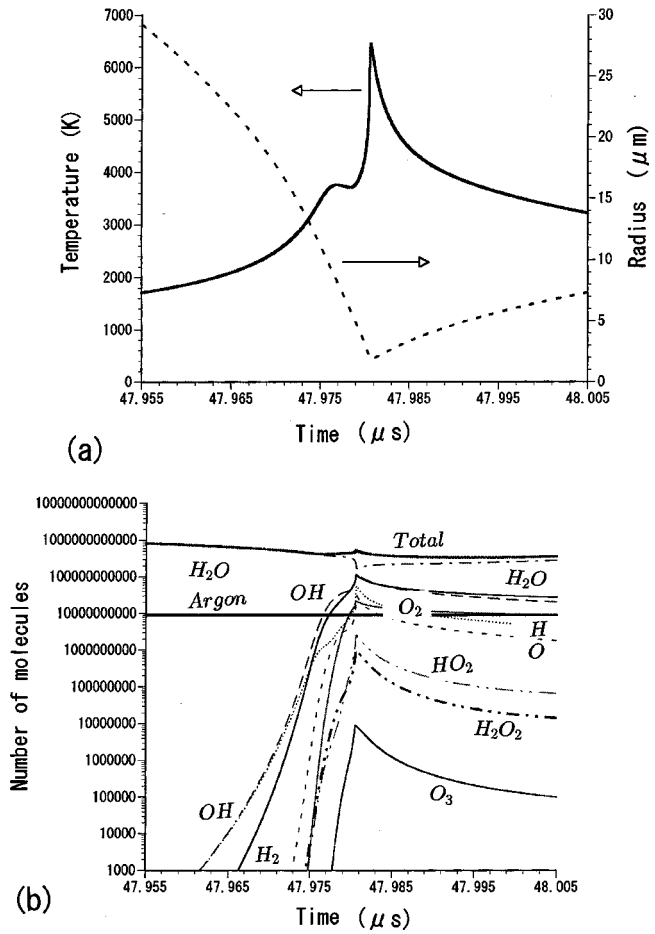

FIG. 9. The calculated results for the liquid temperature of 20 °C at around the minimum bubble radius as functions of time for 0.05 μs. The condition is the same as that of Fig. 8. (a) The bubble radius (R) and the temperature inside the bubble (T). (b) The numbers of molecules inside the bubble.

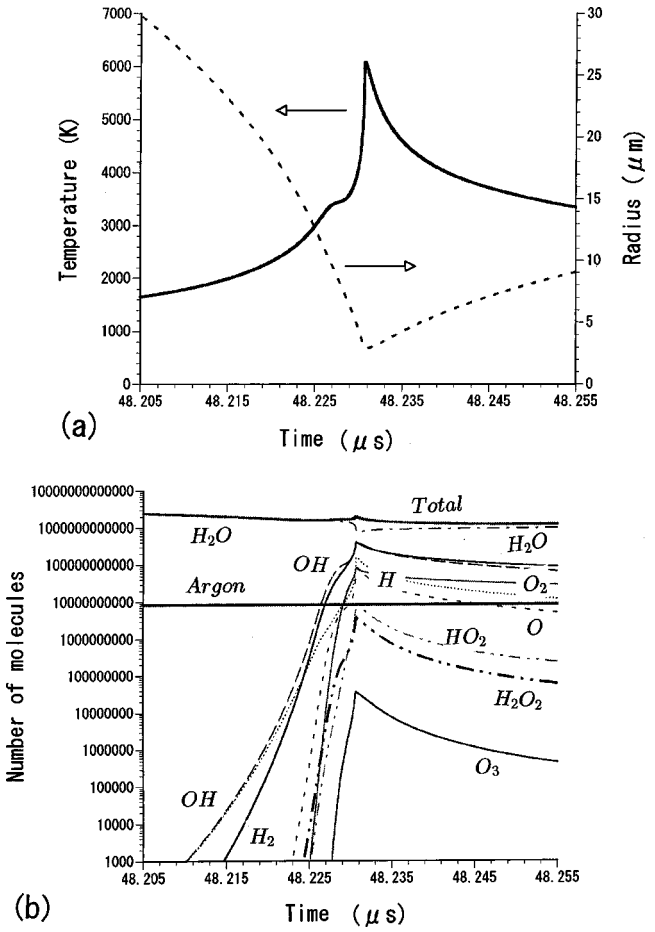

FIG. 10. The calculated results for the liquid temperature of 34 °C at around the minimum bubble radius as functions of time for 0.05 μs. The condition is the same as that of Fig. 8. (a) The bubble radius (R) and the temperature inside the bubble (T). (b) The numbers of molecules inside the bubble.

stronger than those in a hotter liquid due to the higher bubble temperature at the collapse, while chemiluminescence of OH is weaker than that in a hotter liquid. Due to the stronger plasma emissions in a colder liquid, MBSL from a colder liquid is brighter than that from a hotter liquid as reported in many experiments [5–8]. The liquid-temperature dependence of SBSL reported by Vazquez and Putterman [4] is also understood by the difference of the amount of water vapor trapped inside a bubble at the collapse; SBSL from colder liquid is brighter due to the higher maximum bubble temperature because a smaller amount of vapor is trapped inside a bubble at the collapse.

ACKNOWLEDGMENTS

The author thanks Dr. S. Hatanaka, Mr. T. Tuziuti, and Dr. H. Mitome for useful discussions. This study was supported by Special Coordination Funds for Promoting Science and Technology from the Japanese Science and Technology Agency.

APPENDIX: THE UPPER BOUND OF THE SPEED OF THE BUBBLE COLLAPSE

It is shown below by the fundamental theory of fluid dynamics [18] that the bubble wall velocity at the collapse never exceeds the sound velocity in the liquid *at the bubble wall* ($c_{L,B}$).

Consider a liquid flow with no friction. According to the Euler equation,

$$u du = -\frac{dp}{\rho} = -\frac{dp}{d\rho}\frac{d\rho}{\rho} = -c^2\frac{d\rho}{\rho}, \tag{A1}$$

where u is the velocity of the liquid, p is the pressure, ρ is the density, and c is the sound velocity ($c^2 = dp/d\rho$). Using the Mach number $M = u/c$, Eq. (A1) becomes

$$\frac{d\rho}{\rho} = -M^2\frac{du}{u}. \tag{A2}$$

On the other hand, the continuity of fluid (liquid) requires

TABLE III. The calculated results for an argon bubble in water irradiated by ultrasound of 20 kHz and 5 bar for the liquid temperatures of 20 and 34 °C. The ambient bubble radius is 4 μm. ''chemiluminescence'' is that of OH[$OH^* \rightarrow OH + h\nu(310\,nm)$].

	20 °C	34 °C
R_{max}	363 μm	366 μm
R_{min}	1.9 μm	2.9 μm
T_{max}	6500 K	6100 K
(without CR)	(22 000 K)	(18 000 K)
H_2O dissociated	4.6×10^{10}	7.9×10^{10}
light	0.6 pJ	1.7 pJ
pulse width	440 ps	730 ps
mechanism	chemiluminescence	chemiluminescence

$$\frac{d\rho}{\rho}+\frac{du}{u}+\frac{dA}{A}=0, \tag{A3}$$

where A is the cross section of the liquid flow perpendicular to the flow direction [18]. From Eqs. (A2) and (A3),

$$\frac{du}{u}=-\frac{dA/A}{1-M^2}. \tag{A4}$$

From Eq. (A4), it is required that when $M>1$, the cross section must increase ($dA>0$) if the fluid velocity increases ($du>0$). At the bubble collapse, the velocity of the liquid increases towards the bubble [1], which is required by the fluid (liquid) continuity. Thus, for $M>1$, the cross section should increase. However, the cross section of the liquid flow decreases towards the bubble due to the spherically contracting geometry. Thus, it is concluded that M never exceeds 1; in other words, the liquid velocity never exceeds the sound velocity of the liquid. It implies that the speed of the bubble collapse, which is the liquid velocity at the bubble wall, never exceeds the sound velocity of the liquid at the bubble wall.

TABLE IV. The calculated results under the conditions of the experiment by Vazquez and Putterman [4]. The acoustic amplitude (p_a) is determined to reproduce the experimentally observed maximum bubble radius ($R_{max}=37\,\mu$m). The ambient bubble radius is 5 μm. f_a is the frequency of ultrasound used in the experimental [4], ''photons'' is the number of photons emitted per bubble collapse, and the experimentally observed values [4] are given in square brackets.

	20 °C	34 °C
f_a	33.8 kHz	34.3 kHz
p_a	1.32 atm	1.29 atm
T_{max}	10 300 K	9900 K
(without CR)	(11 700 K)	(12 000 K)
H_2O dissociated	1.5×10^{8}	1.7×10^{8}
photons	4.2×10^{4}	3.4×10^{4}
[experiment]	$[6.0\times10^{4}]$	$[1.2\times10^{4}]$
mechanism	atom bremss.	atom bremss.

[1] T. G. Leighton *The Acoustic Bubble* (Academic, London, 1994).
[2] W. Lauterborn, T. Kurz, R. Mettin, and C. D. Ohl, Adv. Chem. Phys. **110**, 295 (1999).
[3] B. P. Barber, R. A. Hiller, R. Löfstedt, S. J. Putterman, and K. R. Weninger, Phys. Rep. **281**, 65 (1997).
[4] G. E. Vazquez and S. J. Putterman, Phys. Rev. Lett. **85**, 3037 (2000).
[5] S. Hatanaka, K. Yasui, T. Tuziuti, and H. Mitome, Jpn. J. Appl. Phys., Part 1 **39**, 2962 (2000).
[6] Y. T. Didenko, D. N. Nastich, S. P. Pugach, Y. A. Polovinka, and V. I. Kvochka, Ultrasonics **32**, 71 (1994).
[7] P. K. Chendke and H. S. Fogler, J. Phys. Chem. **89**, 1673 (1985).
[8] C. Sehgal, R. G. Sutherland, and R. E. Verrall, J. Phys. Chem. **84**, 525 (1980).
[9] S. Hilgenfeldt, D. Lohse, and W. C. Moss, Phys. Rev. Lett. **80**, 1332 (1998); **80**, 3164(E) (1998).
[10] V. Q. Vuong, M. M. Fyrillas, and A. J. Szeri, J. Acoust. Soc. Am. **104**, 2073 (1998).
[11] C. C. Wu and P. H. Roberts, Phys. Rev. Lett. **70**, 3424 (1993).
[12] W. C. Moss, D. B. Clarke, J. W. White, and D. A. Young, Phys. Fluids **6**, 2979 (1994).
[13] K. Yasui, Phys. Rev. E **56**, 6750 (1997).
[14] H. Cheng, M. Chu, P. Leung, and L. Yuan, Phys. Rev. E **58**, R2705 (1998).
[15] L. Yuan, H. Cheng, M. Chu, and P. Leung, Phys. Rev. E **57**, 4265 (1998).
[16] V. Q. Vuong, A. J. Szeri, and D. A. Young, Phys. Fluids **11**, 10 (1999).
[17] K. Yasui, Phys. Rev. E **58**, 4560 (1998).
[18] P. K. Kundu, *Fluid Mechanics* (Academic, San Diego, 1990), p. 594.
[19] B. D. Storey and A. J. Szeri, J. Fluid Mech. **396**, 203 (1999).
[20] Y. S. Touloukian and T. Makita, *Specific Heat* (IFI/Plenum, New York, 1970).
[21] B. D. Storey and A. J. Szeri, Proc. R. Soc. London, Ser. A **456**, 1685 (2000).
[22] R. M. More, J. Quant. Spectrosc. Radiat. Transf. **27**, 345 (1982).
[23] G. B. Zimmerman and R. M. More, J. Quant. Spectrosc. Radiat. Transf. **23**, 517 (1980).
[24] R. Baierlein, *Thermal Physics* (Cambridge University Press, Cambridge, 1999).
[25] R. G. W. Norrish and W. M. Smith, Proc. R. Soc. London, Ser. A **176**, 295 (1940).
[26] T. Carrington, J. Chem. Phys. **30**, 1087 (1959).
[27] L. S. Bernstein, M. R. Zakin, E. B. Flint, and K. S. Suslick, J. Phys. Chem. **100**, 6612 (1996).
[28] R. Mavrodineanu and H. Boiteux, *Flame Spectroscopy* (Wiley, New York, 1965), p. 549.

[29] R. L. Taylor and G. Caledonia, J. Quant. Spectrosc. Radiat. Transf. **9**, 657 (1969).
[30] S. C. Brown, *Basic Data of Plasma Physics* (American Institute of Physics, New York, 1994).
[31] J. C. Keck, J. C. Camm, B. Kivel, and T. Wentink, Jr., Ann. Phys. (Paris) **7**, 1 (1959).
[32] K. Yasui, Ultrasonics **36**, 575 (1998).
[33] K. R. Weninger, C. G. Camara, and S. J. Putterman, Phys. Rev. E **63**, 016 310 (2001).
[34] K. Yasui, J. Acoust. Soc. Am. **98**, 2772 (1995).